Biomedicine & Pharmacotherapy 183 (2025) 117841

Contents lists available at ScienceDirect

Biomedicine & Pharmacotherapy

journal homepage: www.elsevier.com/locate/biopha

Diketopiperazine/piperidine alkaloid as a potential broad-spectrum coronaviral entry inhibitor identified by supercomputer-based virtual screening from a large natural product-based library

Nasim Shahhamzehei [a], Sara Abdelfatah [a], Ejlal A. Omer [a], Max Riedl [b,c], Christian Meesters [b], Hannah S. Schwarzer-Sperber [d], Kathrin Sutter [d,e], Gerhard Bringmann [f], Roland Schwarzer [e,*], Thomas Efferth [a,*]

[a] Department of Pharmaceutical Biology, Institute of Pharmaceutical and Biomedical Sciences, Johannes Gutenberg University, Staudinger Weg 5, Mainz 55128, Germany
[b] HPC-Group, NHR-Southwest, Johannes Gutenberg University, Mainz, Germany
[c] Institute for Medical Informatics, Statistics and Epidemiology, University of Leipzig, Germany
[d] Institute for the Research on HIV and AIDS-associated Diseases (HIV-AAD), University Hospital Essen, University Duisburg-Essen, Essen, Germany
[e] Institute for Virology, University Hospital Essen, University Duisburg-Essen, Essen, Germany
[f] Institute of Organic Chemistry, University of Würzburg, Am Hubland, Würzburg 97074, Germany

ARTICLE INFO

Keywords:
Alkaloids
COVID-19
Natural products
SARS-CoV-2 spike protein
Virtual drug screening

ABSTRACT

The COVID-19 pandemic has underscored the urgent need for antiviral agents capable of targeting a broad range of coronaviruses, including emerging variants of SARS-CoV-2. While vaccines have been pivotal, the search for drugs that can prevent viral entry into host cells remains crucial, especially against evolving viral forms and other coronaviruses. In this study, we investigated natural products as a source of antiviral agents, focusing on their potential to block the spike protein's receptor-binding domain (RBD). Utilizing a library of over 210,000 natural product-based compounds from the ZINC database, we employed a Snakemake workflow to screen for inhibitors against RBDs of SARS-CoV-2, its variants, SARS-CoV, and MERS-CoV. Among top N-heterocyclic candidates from virtual screening we found that one compound, *i.e.*, ((2 *R*,8*S*)-6-(1-benzylpiperidin-4-yl)-2-naphthalen-1-yl-3,6,17-triazatetracyclo[8.7.0.03,8.011,16]heptadeca-1(10),11,13,15 tetraene-4,7-dione), inhibited SARS-CoV-2 pseudovirus and live virus entry in HEK-ACE2 and Vero E6 host cells at low micromolar IC_{50} values. Cell viability assays showed that this compound exerted low cytotoxicity towards HEK-ACE2 while it was not toxic against Vero E6 and MRC5 cell lines. Microscale thermophoresis revealed that this compound strongly bound to the RBDs of SARS-CoV-2, SARS-CoV-2 XBB, SARS-CoV, MERS-CoV, and HCoV-HKU1, with their K_d values increasing as sequence similarity decreased. Molecular docking studies indicated this active compound binds to the SARS-CoV-2 spike protein RBD and interacts with hotspot amino acid residues required for the RBD-ACE2 interaction and cellular infection. These findings show that this diketopiperazine/piperidine-type alkaloid can be considered for further development as a potential pan-coronavirus entry inhibitor.

1. Introduction

The COVID-19 pandemic caused by severe acute respiratory syndrome coronavirus 2 (SARS-CoV-2) had a profound impact on global health, marking the fifth viral pandemic since the 1918 influenza outbreak [1]. Following its first report in Wuhan, China in 2019, it quickly spread around the world with more than 7 million fatalities and close to 776 million reported cases as of September 2024 [2]. While vaccines, monoclonal antibodies, and antiviral drugs have been developed and deployed to curb the spread of SARS-CoV-2, the continuous emergence of new mutant strains, particularly the Omicron subvariants, poses a significant challenge. These variants have demonstrated an increased ability to evade immune detection, reducing the efficacy of existing vaccines and antibody therapies [3,4]. Furthermore, re-infections have a cumulative impact, emphasizing the need for robust and enduring antiviral interventions [5,6]. Current antiviral therapies

* Corresponding authors.
E-mail addresses: Roland.Schwarzer@uk-essen.de (R. Schwarzer), efferth@uni-mainz.de (T. Efferth).

https://doi.org/10.1016/j.biopha.2025.117841
Received 1 October 2024; Received in revised form 3 January 2025; Accepted 10 January 2025
Available online 13 January 2025

for SARS-CoV-2, such as molnupiravir and remdesivir, target the RNA-dependent RNA polymerase (RdRp), while Paxlovid® inhibits the main protease (Mpro). However, these treatments are not without limitations. Concerns about the mutagenic potential of molnupiravir, resistance development to remdesivir, and significant drug-drug interactions with Paxlovid® highlight the need for novel antiviral agents [7]. To date, no small molecule has been approved to target the spike protein, a trimeric structure on the viral surface that plays a vital role in the attachment of the virus and its entry into host cells. Notably, no approved small molecule currently targets the spike protein, a key component responsible for viral attachment and entry into host cells. The spike protein, a trimeric structure, consists of two subunits S1 and S2, each with distinct domains crucial for its function [8]. The receptor-binding domain (RBD) within the S1 subunit plays a pivotal role in binding to the angiotensin-converting enzyme 2 (ACE2) receptor on host cells, facilitating viral entry [9]. Given the central role of the spike protein RBD in the viral infection process, it represents a promising target for therapeutic intervention.

Natural products have demonstrated substantial potential as antiviral agents against SARS-CoV-2 and related respiratory viruses. Several bioactive compounds, including flavonoids, terpenoids, alkaloids, and phenolics, have shown inhibitory effects on key viral targets such as the main protease (Mpro), papain-like protease (PLpro), and the receptor-binding domain (RBD) of the spike protein. For instance, hypericin has demonstrated broad-spectrum inhibitory activity against the main protease (Mpro) of coronaviruses[10]. EGCG, the most active compound extracted from green tea and betulinic acid, is reported to blocks the binding and attachment of the RBD to the ACE2 receptor, reducing the infection rate, inhibiting virus infections[11]. Drug discovery and development remain costly and time-intensive endeavors [12]. Recent advances in computer-aided drug discovery (CADD) offer a solution to expedite this process, particularly through *in silico* screening methods that have proven invaluable during the COVID-19 pandemic [13]. These approaches allow for the rapid identification and optimization of potential drug candidates, significantly reducing the time and costs associated with traditional drug discovery methods. In this study, we employed a high-throughput *in silico* screening approach using a Snakemake workflow on the high-performance computing cluster "Mogon II" [14,15]. This automated, reproducible workflow enabled the efficient screening of over 210,000 natural product-based small molecules from the ZINC database against the RBD of the SARS-CoV-2 spike protein, its variants, SARS-CoV, and MERS-CoV. Following virtual screening, we conducted *in vitro* experiments to evaluate the top candidates' efficacy, aiming to develop a broad-spectrum entry inhibitor against the coronavirus family. This approach ensured automated, highly reproducible execution, facilitating the efficient screening of 210,541 natural-based small molecules from the ZINC database against the receptor-binding domain (RBD) of the spike protein of SARS-CoV2, its variants, SARS-CoV1, and MERS-CoV. Subsequently, we tested the top candidates through various *in vitro* experiments to develop a pan-entry inhibitor against the coronavirus family.

2. Materials and methods

2.1. Cell lines

Human embryonic kidney cells (HEK-ACE2) were purchased from ATCC (American Type Culture Collection, Virginia, USA). The HEK 293 T cell line was generously provided by Dr. Helen May-Simera (Institute of Molecular Physiology, Johannes Gutenberg University, Mainz, Germany). They were cultured in Dulbecco's Modified Eagle Medium (DMEM) (Gibco, Eggenstein, Germany) supplemented with 10 % fetal bovine serum (FBS) and 1 % penicillin/streptomycin (P/S) (Invitrogen, Darmstadt, Germany). Human fetal lung fibroblast cells (MRC-5) were acquired from Dr. Sebastian Zahnreich (Department of Radiation Oncology and Radiation Therapy, University Medical Center of the Johannes Gutenberg University, Mainz, Germany) and cultured in DMEM, low glucose, pyruvate medium with 15 % FBS, 1 % P/S, and 1 % MEM. Non-essential amino acids (Thermo Fisher, Dreieich, Germany) were used for cultivation. Vero E6 cells were obtained from ATCC and cultured in DMEM supplemented with 10 % FBS, 1 % L-glutamine (Capricorn Scientific, Epsdorfergrund, Germany), and 1 % P/S. All cell lines were incubated in a humidified atmosphere at 37 °C and 5 % CO_2.

2.2. Compounds

The top 30 compounds selected from virtual screening were purchased from Vitas M Chemical (Hong Kong SAR, China). The compounds had a purity of $>$ 90 %. All compounds were dissolved in DMSO at a concentration of 20 mM and stored at −20 °C.

2.3. Virtual drug screening

Virtual screening and estimation of binding affinities were performed using a Snakemake workflow that implemented automated steps of structural-based screening. The workflow uses Snakemake (version 6.0.5) for the workflow orchestration, Vina LC (version 1.3.0) for structure-based ligand screening, Open Babel (version 3.0.0) to convert chemical data formats, build indices of datasets, search for substructures, and minimize energy, and Biopython (version 1.75) for the preparation of the target structure. Three major steps constituted the presented workflow: First, preprocessing including, downloading library of 210,541 natural product-based compounds, downloading the target structures (SARS-CoV-2 PDB ID: 7CWM) and preparing ligands by removing error causing structures and energy minimization, removing unwanted structures from the target files and converting those to pdbqt file format and providing the grid box file for the target structures, screening and postprocessing. Second, screening: After preparing the protein structures and compounds using the programs implemented in the workflow, the actual screening takes place. First, only the spike protein of SARS-CoV2 (PDB ID: 7CWM) is screened. The top 30 % of the results, based on their lowest binding energy (cutoff value −8 kcal/mol), are then re-screened with the spike protein of the variants of concern for SARS-CoV-2 (D614G) PDB ID: 7bnn, Epsilon variant PDB ID: 7n8h, Gamma variant PDB ID: 7m8k, Beta variant (B.1.351) PDB ID: 7lyn, Alpha variant (B.1.1.7) PDB ID:7edf, the Swiss model was used to model the spike protein of Delta and Mu variants, as well as SARS-CoV1 (PDB ID:6acd) and MERS-CoV (PDB ID:6nb03).

2.4. Plasmids

To produce pseudoviruses, the following plasmids were obtained from BEI Resources (Littleton, CO, USA): pHAGE-CMV-Luc2-IRES-ZsGreen-W (Cat. # NR-52516), HDM-Hgpm2 (Cat. # NR-52517), HDM-tat1b (Cat. # NR-52518), pRC-CMV-Rev1b (Cat. # NR-52519), pHAGE2-CMV-ZsGreen-W (Cat. # NR-52520), and HDM-IDTSpike-fixK-HA-tail (Cat. # NR-53765). The plasmids were amplified using One Shot™ TOP10 chemically competent *E. coli* (Invitrogen, Thermo Fisher,) and subsequently extracted and purified using the Plasmid Plus Maxi Kit (QIAGEN, Hilden, Germany) to generate a working stock.

2.5. Production of SARS-CoV-2 pseudoviruses and titration

HEK 293 T cells were cultured in DMEM medium supplemented with 10 % FBS to reach 70–80 % confluency the following day. The cells were transfected 24 h post-seeding using Lipofectamine™ 2000 transfection reagent (Invitrogen, Thermo Fisher) with 1 μg of the Luciferase IRES ZsGreen (NR-52516) backbone, along with 0.22 μg each of the plasmids HDM-Hgpm2 (NR-52517), pRC-CMV-Rev1b (NR-52519), and HDM-tat1b (NR-52518), and with or without 0.34 μg of SARS-CoV-2 spike (NR-53765) as a negative control. At 18 h post-transfection, the medium was replaced with fresh DMEM. Supernatants were collected at 48 and

72 h post-transfection, centrifuged at 1250 rpm for 3 min, and stored at −80 °C. For pseudovirus titration, HEK-ACE2 cells were seeded at a density of 12,500 cells per well in white 96-well plates (Cat. # 655074; Greiner, Frickenhausen, Germany). A serial dilution of spike-pseudotyped Luciferase IRES ZsGreen virus was prepared 24 h later, starting from undiluted virus and making six 1:2 dilutions. Then, 24 h after infection, the cell supernatants were replaced with 50 µl of fresh medium per well, followed by the addition of 50 µl of Bright-Glo Luciferase Assay reagent (E2610; Promega, Walldorf, Germany). The cells were incubated for 2 min at room temperature. The luciferase activity was then measured using an Infinite M2000™ Pro plate reader (Tecan, Crailsheim, Germany). The luciferase activity, expressed as relative light units (RLU) *versus* virus dilution, was plotted. The amount of pseudovirus selected for further assays exhibited a signal intensity over 10,000-fold above the cell-only background and was within the linear range of the curve [16,17]. Bald virus expressing no viral spike protein were used as a negative control.

2.6. Pseudovirus inhibition assay

HEK-ACE2 cells (12,500 cells/well) were seeded in white 96-well plates (Greiner, Cat. #655074) 1 d prior to infection. The next day, pseudoviruses were incubated at 37 °C for 1.5 h with either 30 µM of the test compounds or DMSO before being added to the cells. At 24 h post-infection, the medium was replaced with 50 µl of fresh medium per well, followed by the addition of 50 µl of Bright-Glo Luciferase reagent (E2610, Promega). The plates were incubated in the dark at room temperature for 2 min, and luminescence was measured using an Infinite M2000 Pro™ plate reader (Tecan) with a luminescence integration time of 1 sec. Compounds that exhibited more than 50 % inhibitory activity at 30 µM were selected for subsequent dose-response studies, ranging from 0 to 30 µM. Etravirine was used as a positive control [18]. The percentage of infection was calculated using the formula: % infection = [(mean RLU from each sample (virus + compound) - mean RLU from negative cell control) / (mean RLU from virus control - mean RLU from negative cell control)] × 100. The percentage of infection *versus* the log concentration of the inhibitors was used to calculate IC_{50} values [16,17]. For a confirmatory assay, fluorescence microscopy was performed using EVOS digital inverted microscope (Life Technologies GmbH, Darmstadt, Germany). HEK-ACE2 cells (10,000 cells/well) were plated in black 96-well plates (Greiner, Cat. #655936) 1 d before infection. On the day of infection, pseudoviruses were incubated at 37 °C for 1.5 h with 5 µM test compounds or DMSO. At 72 h post-infection, GFP fluorescence was quantified EVOS digital inverted microscope (Life Technologies GmbH, Darmstadt, Germany) and the results were analyzed using ImageJ.

2.7. SARS-CoV-2 propagation and quantification

A SARS-CoV-2 isolate (referred to as the "Essen isolate") derived from patient material, was utilized for infection experiments following the protocol described previously [19]. Vero E6 cells were seeded at a concentration of 2×10^6 cells in a T75 flask and incubated for 24 h at 37 °C with 5 % CO_2 in DMEM supplemented with 10 % FBS, 1 % L-glutamine, 1 % penicillin, and 1 % streptomycin. Subsequently, the cells were infected with the isolated virus and maintained for an additional 72 h under the same conditions. The culture supernatant was then clarified by centrifugation and stored at −80 °C. Viral concentrations were determined using an endpoint dilution assay to quantify the 50 % tissue culture infective dose ($TCID_{50}$). All experiments with infectious SARS-CoV-2 isolates were conducted under BSL3 conditions at the Institute of Virology of the University Hospital Essen, Germany.

2.8. SARS-CoV-2 in-cell ELISA procedure

Virus infections were quantified using an in-cell ELISA method based on a recently published protocol [20]. Cells were seeded at a density of 2×10^4 per well in a flat-bottom 96-well plate 1 d prior to infection. Then, inhibitory compounds were added for at least 30 minutes, prior to infection with SARS-CoV-2 for 24 h. Subsequently, cells were fixed with 4 % paraformaldehyde in phosphate-buffered saline (PBS). Permeabilization was achieved using a 1 % Triton-X-100 solution in PBS, followed by blocking with 3 % fetal calf serum (FCS) in PBS. The primary antibody (Anti-SARS-CoV-2 Nucleocapsid monoclonal antibody ABIN6952435, Antibodies Online, Aachen, Germany) was then added and incubated for 2 h at room temperature. Subsequently, a peroxidase-labeled secondary antibody (Cat. # 115–035–003, Jackson ImmunoResearch, Cambridge, UK) was applied for an additional hour, followed by washing with a 0.05 % Tween-20 solution in PBS. Finally, tetramethylbenzidine (TMB) substrate was added, and the enzymatic reaction was halted using 0.5 M HCl. The absorbance of the resulting dye was measured at 450 nm using a Spark® 10 M multimode microplate reader (Tecan).

2.9. Cell viability assay

Cell viability was evaluated using the resazurin assay, following the protocol previously described [21]. MRC-5 and HEK-ACE2 were seeded in 96-well plates at densities of 2×10^4 cells/well and 1×10^4 cells/well, respectively, and incubated overnight prior to treatment. The following day, cells were exposed to ten different concentrations of compounds ranging from 0.3 to 100 µM. After a 24-h incubation period, 20 µl of 0.01 % resazurin solution (Promega) was added to each well. Fluorescence intensity was measured following a 4-h incubation using an Infinite M2000™ Pro plate reader (Tecan) at an excitation/emission wavelength of 550 nm/590 nm. Cell viability was assessed relative to the DMSO control, with a final concentration of 0.5 % DMSO in the solution. The CC_{50} values, indicating the concentration causing 50 % cytotoxicity, were determined relative to the DMSO-treated control. Each experiment was repeated three times, with six wells per concentration per repetition. Vero E6 cells were seeded at a density of 20,000 cells per well in 96-well plates and incubated overnight. The next day, the cells were exposed to varying concentrations of chemicals. After a 24-h incubation period, the media were replaced with 100 µl of fresh medium. Subsequently, 20 µl of CellTiter-Blue™ reagent (Promega) were added to each well, and the plates were incubated at 37 °C with 5 % CO_2 for 4 h. A Spark® 10 M multimode microplate reader (Tecan) was used to measure fluorescence, exciting the cells at 560 nm and detecting emitted light at 590 nm, to assess cell viability after treatment.

2.10. Sequence alignment

The complete amino acid sequences of the receptor-binding domain (RBD) from the spike proteins of SARS-CoV-2 (P0DTC2), SARS-CoV (P59594), MERS-CoV (K9N5Q8), and HCoV-HKU1 (Q0ZME7) were retrieved from the UniProt database. For the SARS-CoV-2 variant XBB.1, sequences were obtained from the Protein Data Bank (PDB ID: 8iou). Sequence alignment was conducted using Clustal Omega (EMBL-EBI, Wellcome Genome Campus, Hinxton, Cambridgeshire, UK), and graphical representations were generated using Jalview 2.11.3.2 (University of Dundee, Scotland, UK).

2.11. Microscale thermophoresis

The recombinant RBD of spike proteins of SARS-CoV-2, SARS-CoV-2 XBB.1, SARS-CoV, MERS-CoV, and HCoV-HKU1 were obtained from Bio-Techne (Wiesbaden, Germany) to conduct microscale thermophoresis (MST), following established protocols [22,23]. Briefly, these recombinant proteins were labeled using the Monolith Protein Labeling Kit RED-NHS 2nd Generation (MO-L011, Nano Temper Technologies GmbH, Munich, Germany) according to the manufacturer's guidelines. The final protein concentrations post-labeling were 1500 nM for SARS-CoV-2, SARS-CoV-2 XBB.1, and HCoV-HKU1, 1000 nM for

Table 1
Virtual screening results of top 30 natural-derived selected compounds binding to the RBD of spike protein of different coronaviruses.

Compound number	ZINC-ID	Compound-IUPAC name	7CWM SARS-CoV2	7BNN D614G SARS-CoV2	7EDF Alpha Variant	7LYN Beta Variant	7M8K Gamma Variant	Delta Variant	7N8H Epsilon Variant	Mu Variant	6ACD SARS-CoV	6NB3 MERS-CoV
Compound 1	ZINC263586489	(2*Z*,9S)−2-(2,3-dihydro−1,4-benzodioxin−6-ylmethylidene)−9-(7-methyl−2-oxo-1H-quinolin−3-yl)−8,9-dihydrofuro[2,3-*f*]chromene−3,7-dione	−10.8	−11.3	−11.3	−10.5	−11.6	−9.2	−10.5	−9.4	−12.4	−10.3
Compound 2	ZINC253623674	(10 R)−3-(4-chlorophenyl)−5-hydroxy−10-(2-oxo-1H-quinolin−3-yl)−9,10-dihydropyrano[2,3-*h*]chromene−4,8-dione	−10.6	−10.2	−10.3	−9.4	−11.2	−10.8	−10.8	−10.7	−10.2	−11.0
Compound 3	ZINC85876788	(1S,9 R)−11-[[6-[[4-(4-fluorophenyl)−3,6-dihydro-2H-pyridin−1-yl]methyl]−5-hydroxy−1-methyl−4-oxopyridin−2-yl]methyl]−7,11-diazatricyclo [7.3.1.02,7]trideca−2,4-dien−6-one	−10.4	−10.5	−10.6	−9.8	−10.7	−9.4	−10.0	−8.8	−11.0	−10.3
Compound 4	ZINC2104424	(2S,8S)−6-[(2-fluorophenyl)methyl]−2-naphthalen−1-yl−3,6,17-triazatetracyclo[8.7.0.03,8.011,16]heptadeca−1(10),11,13,15-tetraene−4,7-dione	−10.4	−12.0	−9.9	−9.7	−10.7	−9.4	−9.9	−10.0	−10.5	−10.5
Compound 5	ZINC70687282	6-[2-[(4aR,8aS)−4a-hydroxy−1,3,4,5,6,7,8,8a-octahydroisoquinolin−2-yl]−2-oxoethyl]−5,9-dimethyl−3-naphthalen−2-ylfuro[3,2-*g*]chromen−7-one	−10.4	−11.1	−11.2	−9.4	−11.2	−8.7	−11.1	−9.2	−10.9	−11.3
Compound 6	ZINC108450839	(10 R)−5-hydroxy−3-(4-methoxyphenyl)−10-(6-oxo-5H-[1,3]dioxolo[4,5-*g*]quinolin−7-yl)−9,10-dihydropyrano[2,3-*h*]chromene−4,8-dione	−10.3	−10.4	−10.0	−9.9	−11.0	−10.4	−11.9	−10.7	−11.0	−10.6
Compound 7	ZINC15956900	(1S,3 R,3aR,6aS)−1-(1H-indol−3-ylmethyl)−5-naphthalen−2-ylspiro [1,2,3a,6a-tetrahydropyrrolo[3,4-*c*]pyrrole−3,3′-1H-indole]−2′,4,6-trione	−10.3	−11.5	−10.6	−11.7	−11.7	−10.4	−11.1	−9.0	−13.8	−11.8
Compound 8	ZINC85878578	10 R)−5-hydroxy−3-(4-methoxyphenyl)−10-(7-methyl−2-oxo-1H-quinolin−3-yl)−9,10 dihydropyrano[2,3-*h*]chromene−4,8-dione	−10.3	−10.5	−10.4	−9.9	−11.1	−10.2	−11.1	−10.4	−11.0	−10.4
Compound 9	ZINC108447506	(10 R)−5-hydroxy−3-(4-methoxyphenyl)−10-(7-oxo−3,6-dihydro-2H-[1,4]dioxino[2,3-*g*]quinolin−8-yl)−9,10-dihydropyrano[2,3-*h*]chromene−4,8-dione	−10.3	−10.7	−10.4	−9.5	−11.2	−10.5	−11.9	−9.7	−11.3	−11.7
Compound 10	ZINC96114211	(10 R)−5-hydroxy−3-(4-hydroxyphenyl)−10-(7-methyl−2-oxo-1H-quinolin−3-yl)−9,10-dihydropyrano[2,3-*h*]chromene−4,8-dione	−10.2	−10.2	−10.6	−9.6	−11.1	−10.6	−11.4	−10.6	−11.3	−11.6
Compound 11	ZINC883189	(6S,9S)−6-(6-methyl−4-oxochromen−3-yl)−9-phenyl−5,6,8,9,10,11-hexahydrobenzo[*b*][1,4]benzodiazepin−7-one	−10.1	−10.3	−10.5	−10.0	−10.4	−9.3	−9.9	−9.1	−10.3	−11.3
Compound 12	ZINC70706632	(1 R,3 R,3aR,6aS)−5-(4-acetylphenyl)−5′-chloro−1-(1H-indol−3-ylmethyl)−7′-methylspiro[1,2,3a,6a-tetrahydropyrrolo[3,4-*c*]pyrrole−3,3′-1H-indole]−2′,4,6-trione	−10.1	−11.0	−10.5	−9.6	−11.2	−9.1	−10.5	−8.6	−11.8	−11.1
Compound 13	ZINC253401787	(2 R)−10-hydroxy−2-(2-oxo−2-piperidin−1-ylethyl)−6-phenyl−5,13-dioxa−15-azapentacyclo[12.8.0.03,12.04,9.016,21]docosa1(22),3(12),4(9),6,10,14,16,18,20-nonaen−8-one	−10.1	−10.5	−11.5	−10.8	−12.3	−10.1	−11.4	−8.9	−10.8	−12.4
Compound 14	ZINC85876098	(10 R)−5-hydroxy−3-(4-methoxyphenyl)−10-(2-oxo-1H-quinolin−3-yl)−9,10-dihydropyrano[2,3-*h*]chromene−4,8-dione	−10.1	−10.8	−10.0	−9.7	−11.1	−10.3	−11.1	−10.2	−10.9	−10.3
Compound 15	ZINC253623643	(2*Z*,9S)−2-(2,3-dihydro−1,4-benzodioxin−6-ylmethylidene)−9-(7-methoxy−2-oxo-1H-quinolin−3-yl)−8,9-dihydrofuro[2,3-*f*]chromene−3,7-dione	−10.1	−10.5	−10.3	−9.3	−10.9	−8.8	−10.4	−8.8	−11.9	−10.3
Compound 16	ZINC70706585	(1 R,3 R,3aR,6aS)−5-(1,3-benzodioxol−5-ylmethyl)−7'-chloro−1-(1H-indol−3-ylmethyl)spiro[1,2,3a,6a-tetrahydropyrrolo[3,4-*c*]pyrrole−3,3'-1H-indole]−2',4,6-trione	−10.0	−10.9	−11.0	−10.7	−11.1	−9.7	−11.4	−9.7	−13.1	−10.9
Compound 17	ZINC253399830	(10 R)−3-(4-chlorophenyl)−10-[2-(dimethylamino)quinolin−3-yl]−5-hydroxy−9,10-dihydropyrano[2,3-*h*]chromene−4,8-dione	−10.0	−11.3	−9.8	−11.0	−11.1	−9.1	−10.4	−9.2	−12.0	−11.4
Compound 18	ZINC11867127	6-[2-[(4aR,8aS)−4a-hydroxy−1,3,4,5,6,7,8,8a-octahydroisoquinolin−2-yl]−2-oxoethyl]−5-methyl−3-naphthalen−2-ylfuro[3,2-*g*]chromen−7-one	−10.0	−10.6	12.0	−10.8	−11.6	−10.7	−11.1	−9.3	−11.4	−12.0
Compound 19	ZINC253623842	(10 R)−3-(4-chlorophenyl)−5-hydroxy−10-(7-methoxy−2-oxo-1H-quinolin−3-yl)−9,10-dihydropyrano[2,3-*h*]chromene−4,8-dione	−10.0	−10.1	−9.6	−10.0	−11.4	−10.2	−11.3	−10.5	−10.6	−10.5
Compound 20	ZINC70705159	(1S,3S,3aR,6aS)−5′-chloro−5-(2,3-dihydro−1,4-benzodioxin−6-yl)−1-(1H-indol−3 ylmethyl)spiro[1,2,3a,6a-tetrahydropyrrolo[3,4-*c*]pyrrole−3,3′-1H-indole]−2′,4,6-trione	−10.0	−11.1	−11.1	−9.2	−10.7	−9.0	−10.3	−8.6	−11.4	−10.9
Compound 21	ZINC8792352	10-[4-(3chlorophenyl)piperazine−1-carbonyl]−1,11 diazapentacyclo [10.7.1.02,7.08,20.013,18]icosa−2,4,6,8,10,12(20),13,15,17-nonaen−19-one	−10.0	−10.4	−10.6	−10.1	−11.2	−9.5	−11.1	−9.2	−12.2	−11.3

(*continued on next page*)

Table 1 (*continued*)

Compound number	ZINC-ID	Compound-IUPAC name	7CWM SARS-CoV2	7BNN D614G SARS-CoV2	7EDF Alpha Variant	7LYN Beta Variant	7M8K Gamma Variant	Delta Variant	7N8H Epsilon Variant	Mu Variant	6ACD SARS-CoV	6NB3 MERS-CoV
Compound 22	ZINC253401049	2-[5-[(10 R)−3-(4-chlorophenyl)−5-hydroxy−4,8-dioxo−9,10-dihydropyrano[2,3-*h*]chromen−10-yl]furan−2-yl]benzoic acid	−9.9	−10.9	−11.0	−10.5	−11.4	−9.9	−11.6	−10.1	−11.0	−10.8
Compound 23	ZINC70701640	(2 R,11S)-N-[(2S)−1-[(2-chloro−6-fluorophenyl)methylamino]−3-methyl−1-oxobutan−2-yl]−9-oxo−10,20diazapentacyclo[11.7.0.02,10.03,8.014,19]icosa−1(13),3,5,7,14,16,18-heptaene−11-carboxamide	−9.9	−10.2	−10.8	−10.7	−11.5	−8.9	−9.9	−8.5	−10.5	−10.6
Compound 24	ZINC19782240	2-[[(6S)−10,10-dimethyl−9-oxa−2-azaspiro[5.5]undecan−2-yl]methyl]spiro[3,6-dihydrobenzo[*h*]quinazoline−5,1′-cyclohexane]−4-one	−9.9	−10.7	−10.7	−10.1	−11.2	−9.9	−10.9	−8.8	−11.0	−13.0
Compound 25	ZINC104739723	6-[3-[(4aR,8aS)−4a-hydroxy−1,3,4,5,6,7,8,8a-octahydroisoquinolin−2-yl]−3-oxopropyl]−5-methyl−3-naphthalen−2-ylfuro[3,2-*g*]chromen−7-one	−9.9	−10.5	−10.7	−9.8	−10.8	−9.8	−10.7	−9.1	−11.6	−10.7
Compound 26	ZINC70670218	(5 R)−1-benzyl−5-(naphthalen−1-ylmethyl)−5-[[(1S,9 R)−6-oxo−7,11diazatricyclo[7.3.1.02,7]trideca−2,4-dien−11-yl]methyl]−1,3-diazinane−2,4,6-trione	−9.9	−11.1	−10.9	−10.7	−11.7	−9.6	−10.3	−8.5	−12.4	−11.3
Compound 27	ZINC85878218	3-[3-(4-benzo[*b*][1,4]benzoxazepin−6-yl)piperazin−1-yl)−3-oxopropyl]−3,13,21triazapentacyclo[11.8.0.02,10.04,9.015,20]henicosa−1(21),2(10),4,6,8,15,17,19-octaen−14-one	−9.9	−11.6	−11.4	−11.8	−12.9	−9.5	−11.8	−10.3	−11.7	−11.4
Compound 28	ZINC70686498	(2 R,8S)−6-(1-benzylpiperidin−4-yl)−2-naphthalen−1-yl−3,6,17-triazatetracyclo[8.7.0.03,8.011,16]heptadeca−1(10),11,13,15-tetraene−4,7-dione	−9.9	−11.7	−11.0	−11.6	−11.8	−10.6	−10.9	−8.9	−11.3	−10.7
Compound 29	ZINC70699829	(1S,3 R,3aR,6aS)−5-(2,3-dihydro−1,4-benzodioxin−6-yl)−1-(1H-indol−3-ylmethyl)−6′,7′-dimethylspiro[1,2,3a,6a-tetrahydropyrrolo[3,4-*c*]pyrrole−3,3′-1H-indole]−2′,4,6-trione	−9.9	−10.3	−10.3	−9.7	−11.3	−8.7	−10.9	−8.3	−10.5	−10.3
Compound 30	ZINC11867100	3-[2-[(4aS,8aR)−4a-hydroxy−1,3,4,5,6,7,8,8aoctahydroisoquinolin−2-yl]−2-oxoethyl]−4,8-dimethyl−7-[(2-methylnaphthalen−1-yl)methoxy]chromen−2-one	−9.9	−10.4	−10.0	−10.2	−10.8	−8.9	−11.2	−9.1	−10.2	−10.4

SARS-CoV, and 750 nM for MERS-CoV (Nanodrop, Thermo Fisher Scientific). Titration was performed using 16 serial dilutions, ranging from 200 to 0.006 M concentration (dilution steps 1:1). Titration involved 16 serial dilutions ranging from 200 to 0.006 M (1:1 dilution steps). The ligand and protein were incubated for 30 min at room temperature in an assay buffer containing 50 mM Tris (pH 7.4), 10 mM $MgCl_2$, 150 mM NaCl, and 0.05 % Tween-20. Measurements were performed using Monolith NT.115 standard capillaries (MO-K022, Nano Temper Technologies GmbH, Munich, Germany) with laser power settings of 10 %, 20 %, 40 %, and 60 %, and an LED power at 20 % for MERS-CoV, HCoV-HKU1, and 30 % for SARS-CoV-2, SARS-CoV-2 XBB.1, and SARS-CoV. Signals were measured with the Monolith NT.115 instrument (Nano Temper Technologies). Fitting curves and Kd values were determined using NT Analysis 1.5.41 software (Nano Temper Technologies).

2.12. Molecular docking

The most promising compound identified from initial *in vitro* experiments (compound 28) was subjected to the molecular docking studies against the receptor-binding domains (RBDs) of several coronaviruses: SARS-CoV-2 (PDB ID: 7bnn), SARS-CoV-2 XBB.1 (PDB ID: 8iou), SARS-CoV (PDB ID: 6acd), MERS-CoV (PDB ID: 6nb03), and HCoV-HKU1 (PDB ID: 8opo). AutoDock 4.2.6 was employed in a defined docking mode using the Lamarckian algorithm. The protein was kept rigid, while the ligand moved during the docking simulation. The parameters were set to 250 runs and 2,500,000 energy evaluations for each cycle, while the other docking parameters were kept at default values as described by our group [24] to assess the binding affinities and elucidate the amino acid residues critical for interaction within these RBDs. Computational docking simulations were executed on the high-performance supercomputer MOGON at Johannes Gutenberg University (Mainz, Germany). Visualization and interpretation of the docking outcomes were facilitated using Discovery Studio Visualizer V 21.1.0.20298 (San Diego, CA, USA).

2.13. Statistics and data fitting

All inhibition assays were performed at least as duplicates per plate, and all results shown are the average of at least three independent experiments. The binding data were converted to percent infection and fitted with standard log inhibitor *versus* normalized response models (four parameters) using nonlinear regression in GraphPad Prism 8 (GraphPad, La Jolla, CA, USA) to establish half-maximal toxicity or inhibitory concentrations (CC_{50}, IC_{50}). The selectivity index (SI) of an active compound was calculated using: $SI = CC_{50}/EC_{50}$ equation for live and pseudo-typed viruses. The correlation between the Kd values and the percentage of identity of RBDs was determined using Pearson's correlation test.

3. Results

3.1. Virtual screening

Vina LC software was used to run a Snakemake workflow which combined all major aspects of structure-based ligand screening: Automated execution of intricate preparation and screening steps, including retrieval of ligands libraries from databases, optional decompression and energy minimization, protein download from the Protein Data Bank (RCBS) database and protein preparation followed by selection of screening parameters. Screening was performed on a high-performance computer (Mogon II) to screen a ZINC library of 210,541 natural product-based compounds towards the RBD of spike protein of different coronaviruses. The protein binding pocket was identified based on amino acids known to be involved in spike RBD-receptor interactions. For all coronavirus spike proteins under investigation, 626 different compounds had binding energy less than −8 kcal/mol. The top 30

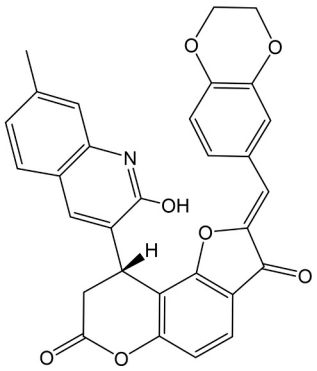

Compound **1**

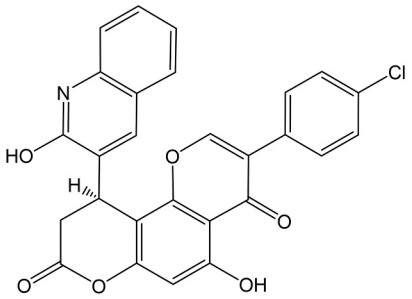

Compound **2**

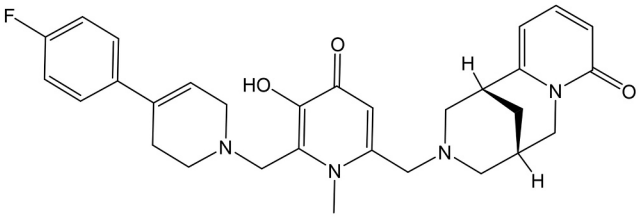

Compound **3**

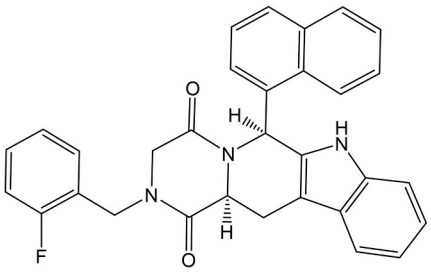

Compound **4**

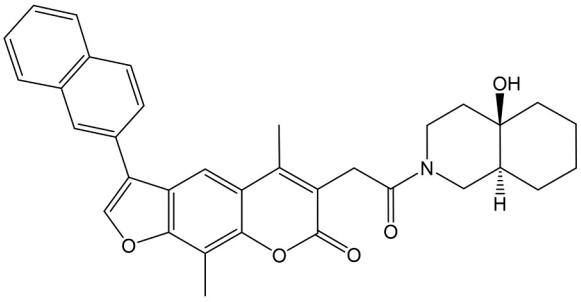

Compound **5**

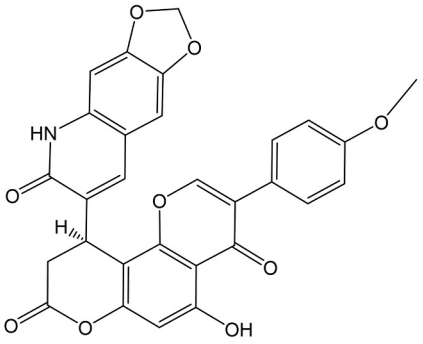

Compound **6**

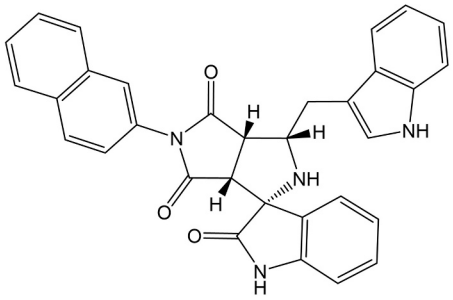

Compound **7**

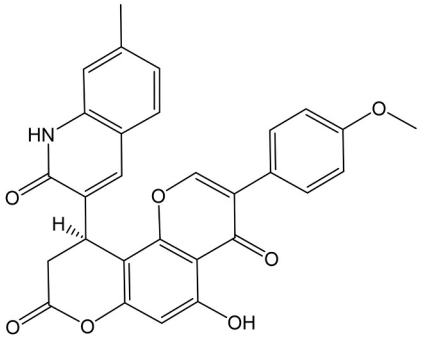

Compound **8**

Fig. 1. Chemical structures of the top 30 natural-derived compounds exhibiting highest binding affinity to the RBD of the SARS-CoV-2 spike protein. The binding affinities are expressed as lowest binding energies (LBE) in kcal/mol obtained.

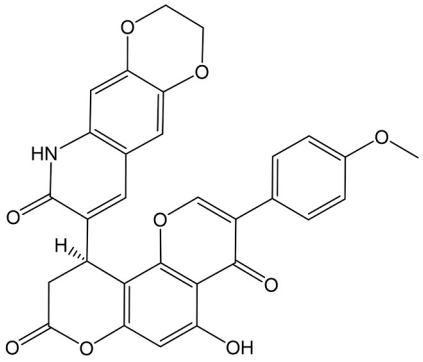

Compound **9**

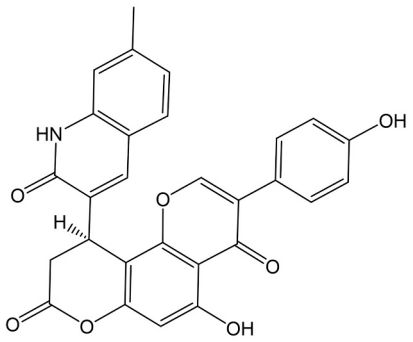

Compound **10**

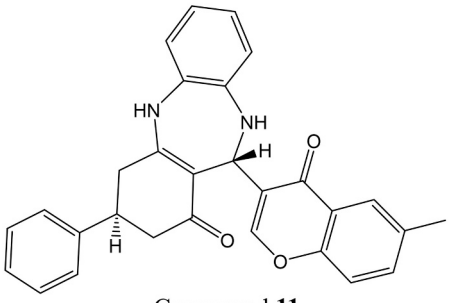

Compound **11**

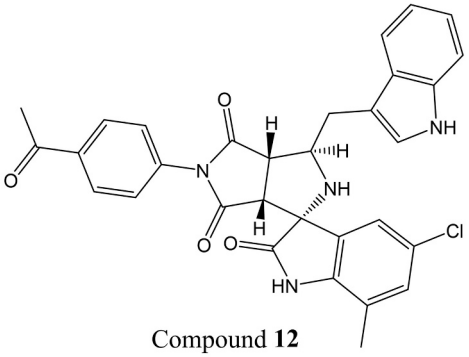

Compound **12**

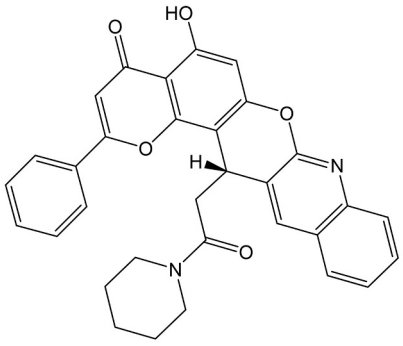

Compound **13**

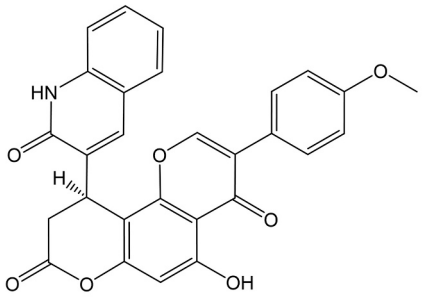

Compound **14**

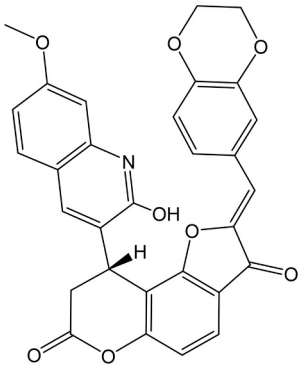

Compound **15**

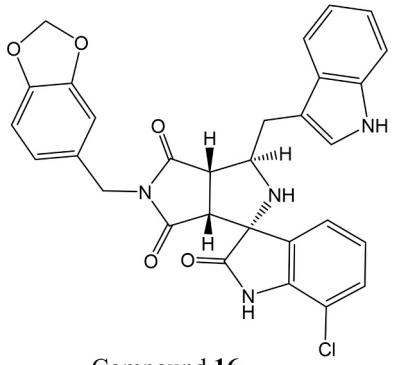

Compound **16**

Fig. 1. (*continued*).

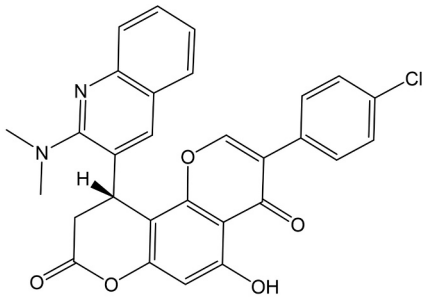

Compound **17**

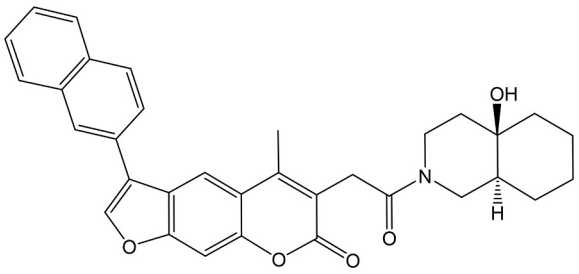

Compound **18**

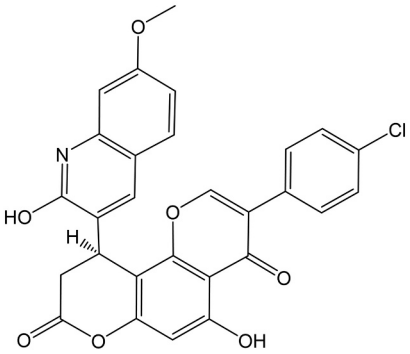

Compound **19**

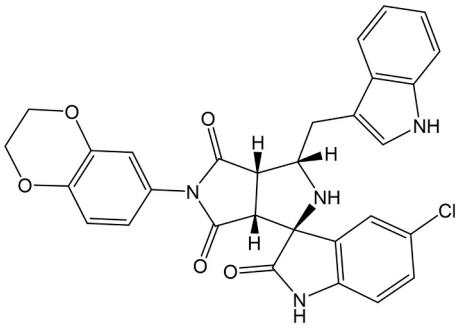

Compound **20**

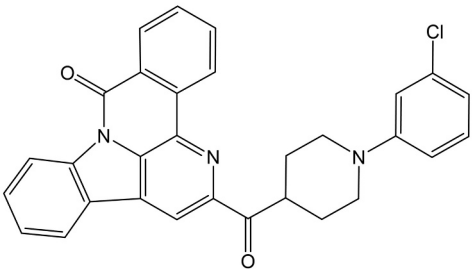

Compound **21**

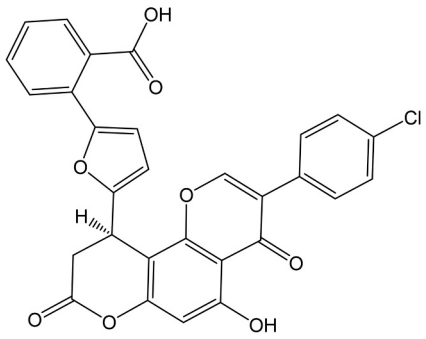

Compound **22**

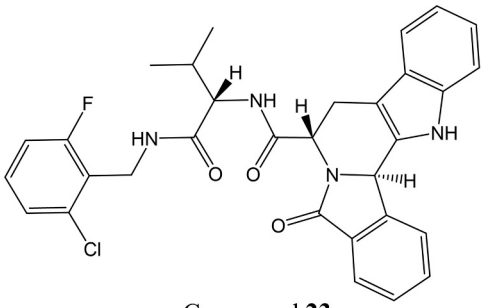

Compound **23**

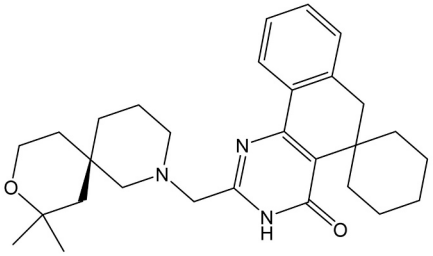

Compound **24**

Fig. 1. (*continued*).

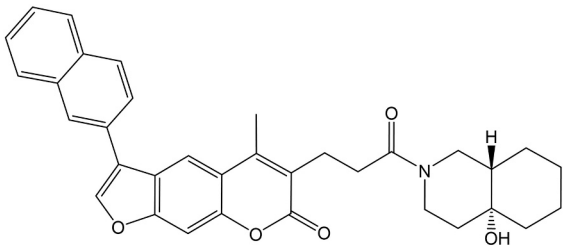

Compound **25**

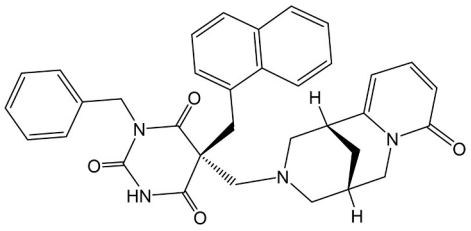

Compound **26**

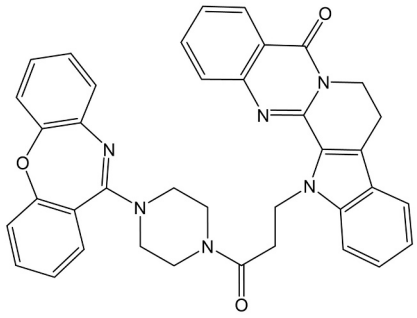

Compound **27**

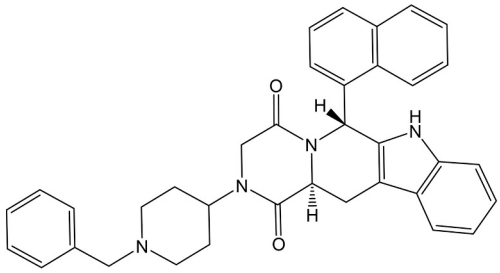

Compound **28**

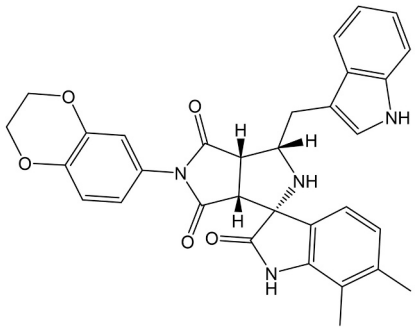

Compound **29**

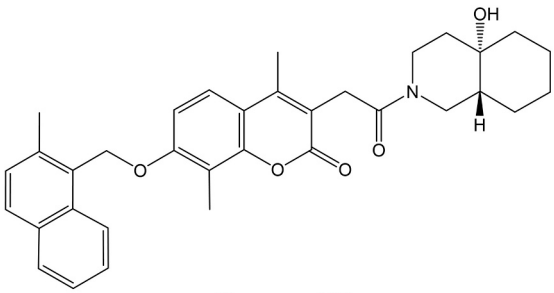

Compound **30**

Fig. 1. (*continued*).

candidates were selected for the *in vitro* experiments (Table 1). The candidates were selected based on their binding affinity to SARS-CoV-2 RBD, prioritizing those with the lowest binding energies. Additionally, the commercial availability of the compounds was a crucial factor in the selection process. The chemical structures of the top 30 compounds are shown in Fig. 1.

3.2. Inhibition of pseudotyped and live SARS-CoV-2 infection

Luciferase assays were conducted in HEK-ACE2 cells to screen the top 30 candidates identified from in silico studies, aiming to discover novel anti-SARS-CoV-2 entry inhibitors. While following the initial screening (Fig. 2A), six compounds (**2**, **6**, **14**, **17**, **19**, and **28**) demonstrated more than 50 % inhibition of pseudovirus entry at the concentration of 30 μM, only compound 28 was subjected to dose-response experiments to determine the concentration required to inhibit pseudovirus entry by 50 % (IC_{50}), since the other compounds showed high toxicity against HEK-ACE2 cells ($CC_{50} \leq 30$) (Table 2). The IC_{50} values for compound **28** was 1.96 ± 0.14 μM (Fig. 2B). GFP fluorescence measured via live fluorescence microscopy revealed that compound **28** provided strong protection against pseudovirus, 72 h after infection, which was consistent with the results from the luciferase inhibition assay (Fig. 2C-D).

The inhibitory efficacy of compound **28** against live SARS-CoV-2 viruses was evaluated through titration assays to determine its IC_{50} value. The result demonstrated that compound **28** inhibited SARS-CoV-2 infection at the cellular level with an IC_{50} value of 5.024 ± 0.53 μM (Fig. 2E).

3.3. Cell viability

The cytotoxicity of compound **28** was tested on MRC-5, HEK-ACE2, and Vero E6 cell lines, using the resazurin assay. The cell viability assay showed that compound **28** was cytotoxic against HEK-ACE2, with a CC_{50} value of 43.4 ± 7.4 while it did not show toxicity towards MRC-5 and Vero E6 cells even in the high concentration (Fig. 3).

3.4. Sequence alignment

To evaluate whether our leading compound can bind to the spike protein of various coronavirus family members, sequence alignments were conducted to assess the similarity between the receptor-binding domains (RBD) of the spike proteins from different coronaviruses. The alignments revealed sequence identities of 89.91 % with SARS-CoV-2

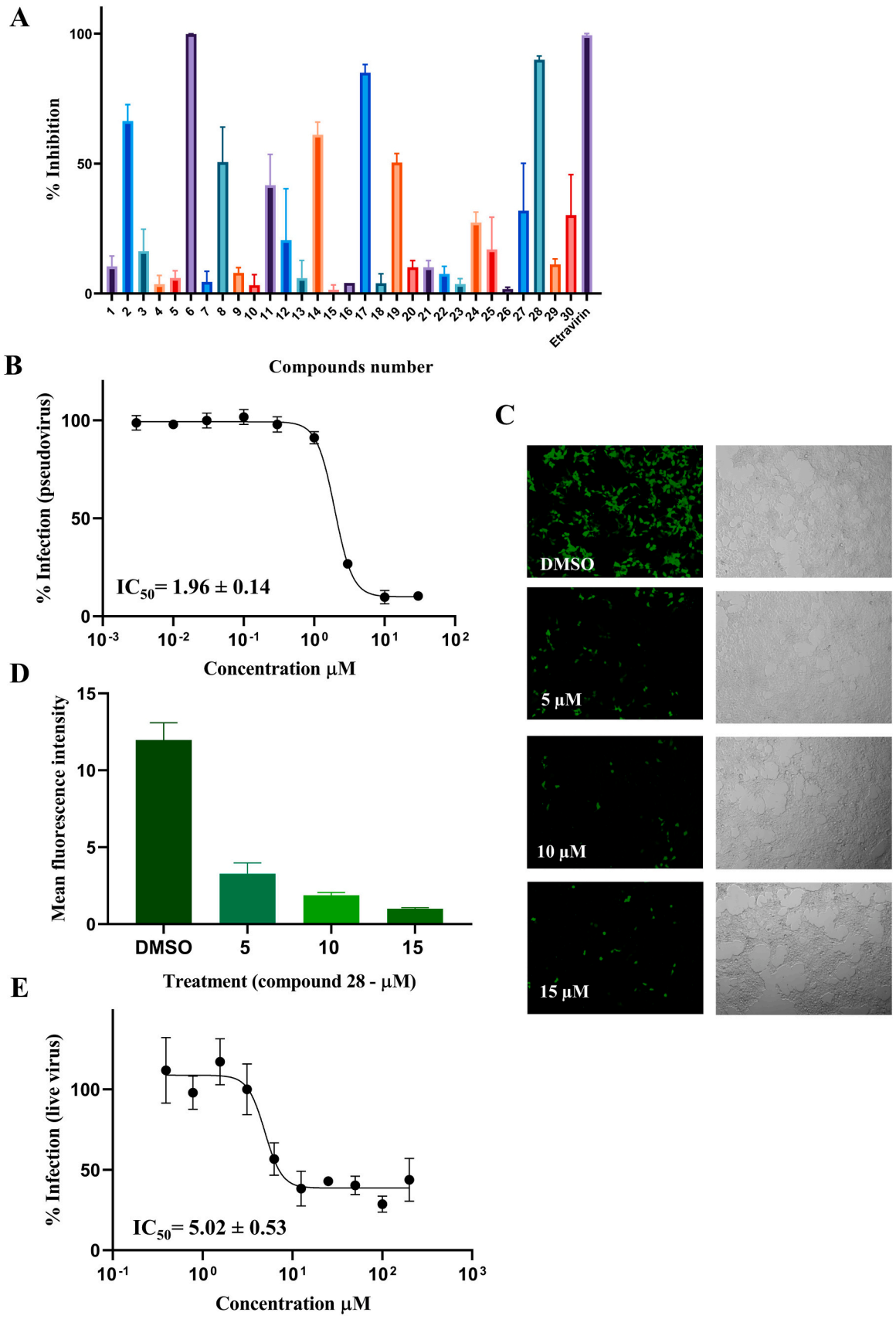

(caption on next page)

Fig. 2. Identification of entry inhibitors against pseudotyped SARS-CoV-2 lentivirus in HEK-ACE2 cells: (A) Percentage of inhibition of the SARS-CoV-2 pseudovirus in the presence of 30 selected natural-derived compounds and etravirine as a positive control (30 μM). (B) Dose-response curves of compound **28** on the SARS-CoV-2 pseudovirus, IC_{50} values and data points are shown as mean ± SD for three independent replicates. (C) Fluorescence microscopic images of HEK-ACE2 treated with pseudotyped SARS-CoV-2 lentivirus in the presence of 0, 5, 10, and 15 μM of compound **28**. (D) Quantification of GFP fluoresces standardized to the mean of fluorescence intensity using Image J, at 0, 5, 10, and 15 μM concentration of compound **28** and presented as mean ± S.D of three replicates. (E) Inhibition of fully replication-competent SARS-CoV-2. Vero E6 cells were infected with a clinical SARS-CoV-2 isolate for 24 h in the presence of compound **28** at the indicated concentrations. Infection levels were quantified by in-cell ELISA and normalized to mock-treated control wells (infected, but non-treated). Infection data were fitted with a four parameters inhibitor vs. response function (Y = Bottom + (Top - Bottom)/(1 + (IC_{50} / X) ^ HillSlope) using the statistics software GraphPad prism. Data points show mean ± standard error of the mean, calculated from at least three independent titrations of each compound.

Table 2
CC_{50} values of seven active compounds from pseudovirus inhibition assay screening, towards HEK-ACE2. The data are plotted as mean values ± SD of three independent experiments.

Compounds ZINC-ID	Compounds number	CC_{50} (μM)
ZINC253623674	**2**	10.86 ± 0.95
ZINC108450839	**6**	2.53 ± 0.44
ZINC85878578	**8**	14.45 ± 2.007
ZINC85876098	**14**	15.16 ± 0.36
ZINC253399830	**17**	18.96 ± 2.83
ZINC253623842	**19**	11.57 ± 1.58
ZINC70686498	**28**	43.40 ± 7.40

XBB.1 (Omicron variant), 73.42 % with SARS-CoV, 18.75 % with MERS-CoV, and 19.81 % with HCoV-HKU1, compared to the SARS-CoV-2 spike RBD. The multiple sequence alignment of the RBD domain of these coronaviruses is shown in Fig. 4, which is colored with the Taylor color scheme. Here, the colors are set by the variation in polarity and size of different amino acid chains. Hydrophobic amino acids are colored green, aromatic amino acids are green-blue, large polar/basic amino acids are purple and blue, amino acids found in loops are orange and red.

3.5. Microscale thermophoresis

As a sensitive technology, microscale thermophoresis was utilized to determine the binding affinity between the compound **28** and the labeled RBD of spike proteins from various coronavirus species, including different SARS-CoV-2 variants, SARS-CoV, MERS-CoV, and the endemic strain HCoV-HKU1. For this purpose, the labeled recombinant RBDs of spike proteins from SARS-CoV-2, SARS-CoV-2 XBB.1, SARS-CoV, MERS-CoV, and HCoV-HKU1 were titrated against varying concentrations of selected compound. Compound 28 bound to the RBD of spike proteins of SARS-CoV-2, SARS-CoV-2XBB.1, SARS-CoV, HCoV-HKU1, and MERS-CoV, with K_d values of 2.96, 4.2, 7.02, 20.08, and 23.06 μM, respectively (Fig. 5).

3.6. Binding mode of the top candidate

Molecular docking studies using AutoDock 4.2.6 revealed that compounds **28** exhibited high binding affinities to the RBD of spike proteins of SARS-CoV-2, SARS-CoV-2 XBB.1, SARS-CoV, MERS-CoV, and HCoV-HKU1, which have the potential to block the binding of RBD to ACE2, thereby protecting healthy cells and preventing further degeneration in the early stages of infection. Compound **28** had low binding energy (LBE) values ranging from −9.66 to −11.09 kcal/mol and predicted inhibition constants (pKi) between 7.36 and 83.56 nM. The amino acid interactions between the candidate compounds and the target proteins are illustrated in Fig. 6.

4. Discussion

During the past two decades, the world has experienced major outbreaks of coronavirus infection that threatened the global health, in 2002–2003 by SARS-CoV and in 2011 by MERS-CoV. The most recent coronavirus outbreak, known as COVID-19, happened in 2019 [25]. Despite the rapid development and deployment of vaccines and FDA-approved small-molecule antivirals, effective prophylactic and treatment options for COVID-19 are still needed to supplement vaccination efforts and ensure preparedness for future coronavirus outbreaks, including future variants against which current vaccines may be less effective.

As such, with the aim of finding novel pan-coronaviral substances, we screened 210,541 natural products using a Snakemake workflow. The 30 compounds identified according to their lowest binding energies (kcal/mol) from the virtual screening are structurally most divergent, but have, all of them, in common the presence of nitrogen atoms (even up to six in the case of compound **27**), all containing *N*-heterocycles, mono- or bicyclic, or even having more complex polycyclic ring systems. In addition, most of the compounds (no less than 21 out of 30) also possess oxygen-containing heterocycles. In 16 cases, there are even several oxygen-heterocycles and/or heterocycles with more than one oxygen atom. But apart from these similarities, the 30 preselected structures are rather characterized by a large structural diversity,

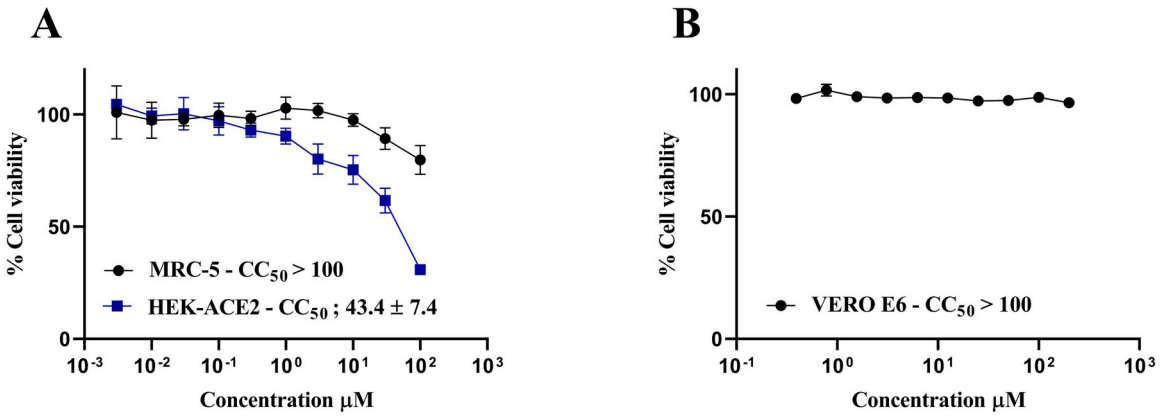

Fig. 3. Cytotoxic effects of compound **28** against (A) HEK-ACE2 and MRC-5 and (B) Vero E6 cell lines. The cytotoxicity was assessed using the resazurin method. Each data point represents the mean value ± SD of three independent experiments with six replicates each.

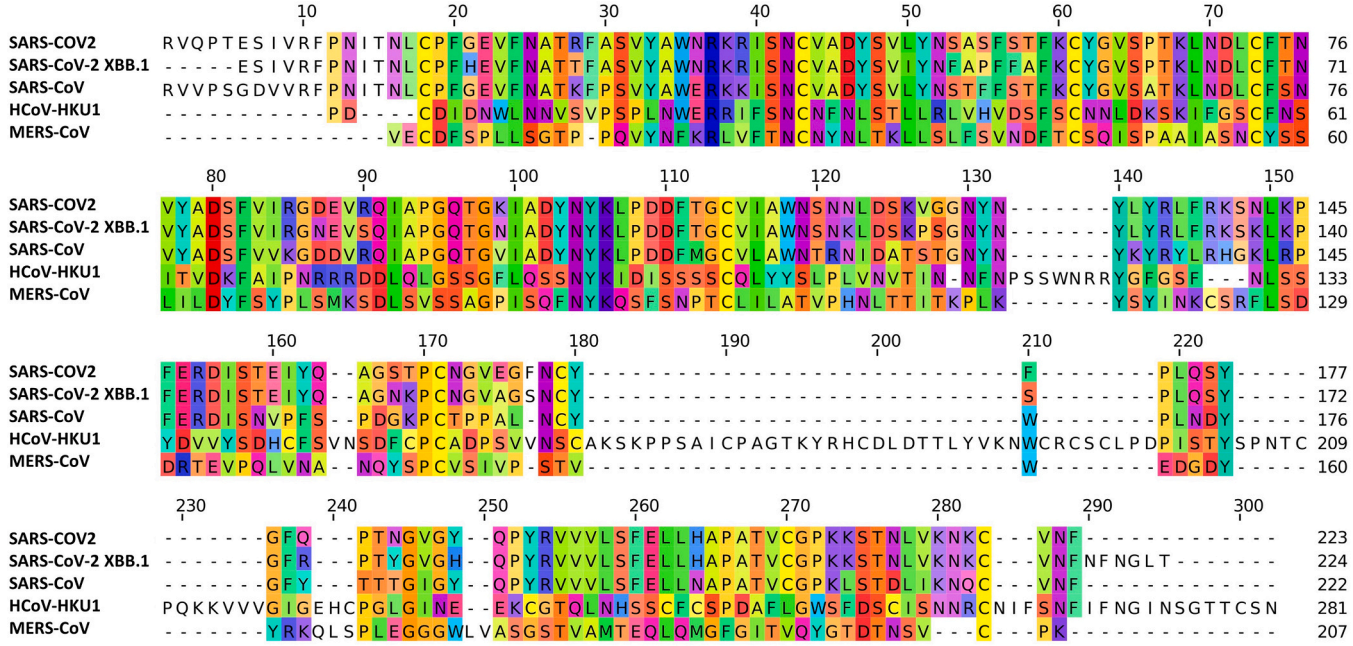

Fig. 4. Multiple sequence alignments of the RBD of spike proteins of SARS-CoV-2, SARS-CoV-2 XBB.1, SARS-CoV, MERS-CoV, and HCoV-HKU1.

making it difficult to find significant structure-activity relationships.

More interesting is a closer look at compound **28**, which is the only one that is active *in vitro* and possesses several types of heterocyclic rings-diketopiperazine, piperidine, and indole units. Compound **28** has its nitrogen in several mono- and bicyclic rings, even forming in a tetracyclic ring system, consisting of a tetrahydroharman (1,2,3,4-tetrahydro-β-carboline) system, fused to the mentioned diketopiperazine. Here, in **28**, the natural amino acid L-tryptophan, as part of an *N*-benzylpiperidine-substituted 2,5-diketopiperazine, has undergone a further Pictet-Spengler-type cyclization with (non-natural) naphthalene-1-carbaldehyde to form a remarkable tetracyclic ring system. In contrast to the other investigated molecules, **28** does not contain any oxygen-heterocycles.

Nitrogen-containing heterocyclic compounds are abundant in nature and serve as the basis for a diverse range of molecules, including alkaloids, vitamins, hormones, dyes, antibiotics, herbicides, and medicines. Notable examples of nitrogen-containing molecules that occur naturally include morphine, caffeine, nicotine, thiamine, and atropine. These compounds are categorized as alkaloids. In addition, *N*-heterocyclic compounds have several biological actions, including antifungal, anti-inflammatory, antibacterial, antioxidant, anticonvulsant, antiallergic, enzyme inhibitory, herbicidal, anti-HIV, antidiabetic, anticancer, and insecticidal properties. Nitrogen-containing heterocycles have long been a central focus of scientific investigation because of their varied structures and biological importance [26].

A recent analysis has shown that 82 % (262 out of 321) of the small-molecule medications that received approval from the FDA between 2013 and 2023 have a nitrogen heterocycle. Out of all the new small-molecule medications, a majority of 89 (28 %) are specifically authorized for cancer therapies. Among them, 55 compounds are classified as kinase inhibitors. The category of anti-infective pharmaceuticals is the second most common in terms of diseases, with 56 (17 %) new drugs. Out of these, ten have been licensed for treating hepatitis C, a remarkable achievement in the field of antiviral drug research [27,28].

Piperidine, a six-membered ring with one nitrogen atom, and piperazine, a six-membered ring with two nitrogen atoms, are prime examples of nitrogen-containing heterocycles [28]. Piperidine itself exhibits tremendous utility in the field of therapeutics [29]. This motif occurs abundantly in nature among alkaloids and exists in many genera including *Nicotiana, Conium, Lobelia, Pinus, Punica, Duboisia, Sedum, Withania, Carica, Hydrangea, Dichroa, Cassia, Prosopis, Genista, Ammodendron, Lupinus, Liparia*, *Ancistrocladus,* and *Collidium*. During the past years, alkaloid-based antiviral therapies have garnered significant attention. Numerous studies have demonstrated that alkaloids can effectively prevent and treat viral infections [30]. Thus, Dongwei et al. developed a series of piperidine derivatives as inhibitors of HIV-1 and influenza A virus replication in cell culture, showing that nearly half of the tested compounds exhibited potent activity against WT HIV-1 in MT-4 cells, with EC_{50} values ranging from 3.93 to 27.33 μM [31]. Similarly, piperidine alkaloids from *Senna spectabilis* flowers have potential for repurposing as anti-Chikungunya virus drugs, with EC_{50} values between 8.3 and 14.9 μM in BHK-21 cells [32].

The *N*-benzyl substitution on piperidine within drug molecules has demonstrated a strong affinity for molecular targets, resulting in its widespread presence as the *N*-benzyl piperidine (NBP) fragment in bioactive compounds. This *N*-benzyl substitution enhances solubility by forming a salt at the tertiary nitrogen and facilitates essential cation-π and π-π interactions with active sites of various targets [33].

Indole diketopiperazine alkaloids are metabolites produced by microbes, predominantly isolated from fungi such as *Aspergillus, Penicillium, Pestalotiopsis*, and *Chromocleista* [34]. These substances are defined by their unique condensation products, which typically involve a complete tryptophan molecule and a second amino acid, such as L-tryptophan, L-proline, L-phenylalanine, L-histidine, or L-leucine, resulting in the formation of an indole diketopiperazine unit [35,36]. The interest in indole diketopiperazines stems from their notable biological activities, including antimicrobial, antiviral, anticancer, immunomodulatory, antioxidant, and insecticidal properties. Consequently, these compounds hold promise for potential drug applications and may serve as valuable lead structures in drug development [36]. During the past decade many studies have highlighted their potential antiviral applications for instance, neoechinulin B, an indole diketopiperazine alkaloid, isolated from *Eurotium rubrum* Hiji025, and its derivatives exhibited antiviral effects against hepatitis C virus (HCV) and SARS-CoV-2 in Huh 7 cell line with the IC_{50} values of 4.9–0.0059 μM and 32.9–6.0 μM, respectively [37]. Additionally, 2,5-diketopiperazine derivatives exhibited negative results in influenza virus propagation at a concentration of 25 μg/ml in embryonated chicken eggs [38]. We first used a

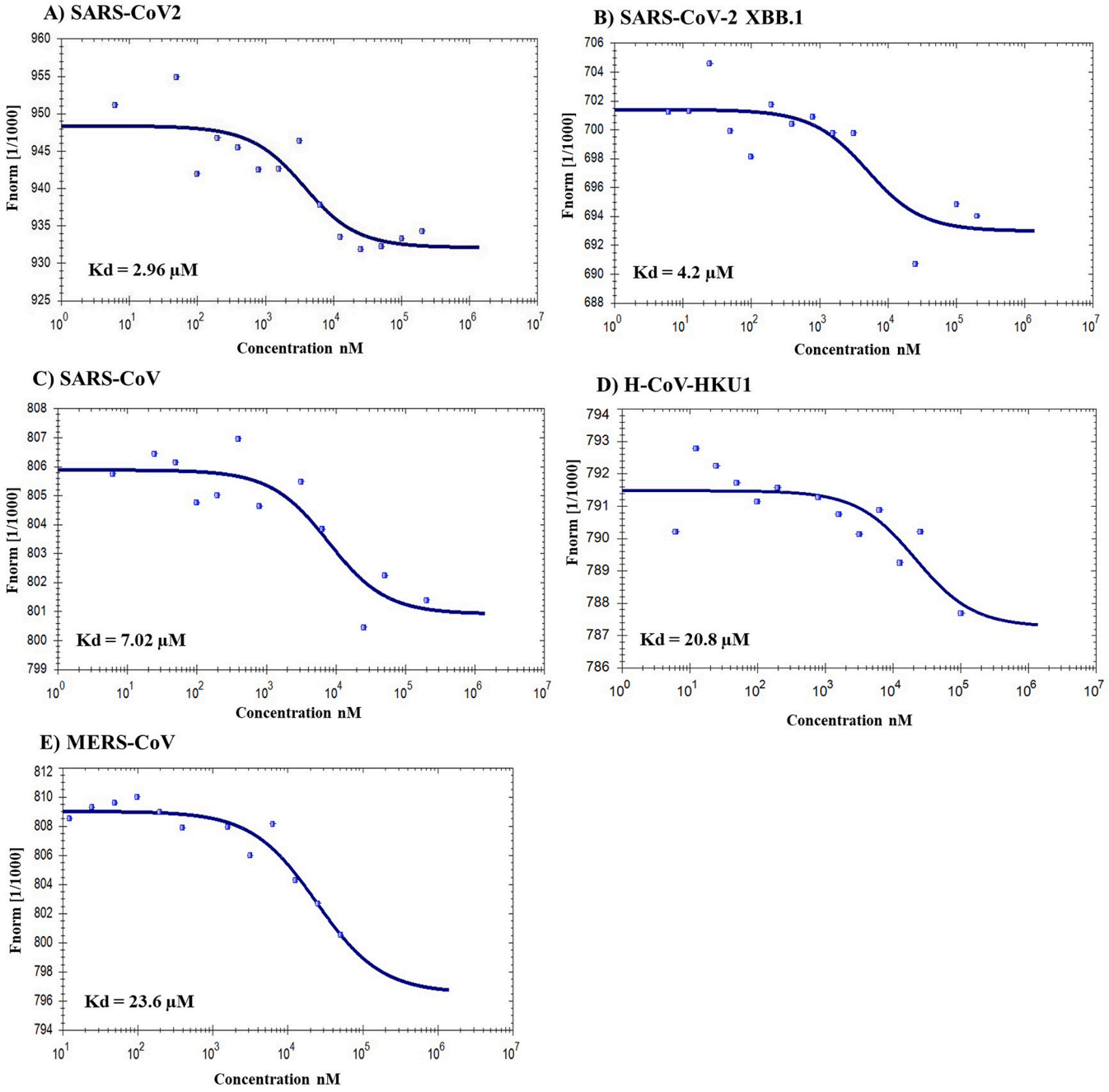

Fig. 5. Microscale thermophoresis analysis of compound **28** with the RBD of spike protein of (A) SARS-CoV-2, (B) SARS-CoV-2 XBB.1, (C) SARS-CoV, (D) H-CoV-HKU1, and /E) MERS-CoV.

pseudovirus technology to screen preselected compounds from virtual screening against the viral entry process in a biosafety level 2 laboratory. The pseudovirus inhibition assays showed that compound **28** strongly inhibits the cellular pseudovirus entry, with a IC_{50} value of 1.96 ± 0.14 µM and a selectivity index of 21.75 in HEK-ACE2. To validate the results of the pseudovirus inhibition assays, the active compound was subjected to the inhibition of live SARS-CoV2 replication assays in a biosafety level 2 laboratory. The results revealed that compound **28** has inhibitory effects against SARS-CoV2 with IC_{50} values of 5.024 ± 0.53 µM. The IC_{50} values from the pseudovirus inhibition assay were lower related to the low titer of pseudovirus compared to the live viruses. Remarkably, the cell viability assays showed that compounds **28** has a very low cytotoxicity against HEK-ACE2, while it is not toxic towards MRC-5 and Vero E6 cell lines.

Up to now, there has been a significant number of studies dedicated to identifying natural chemicals that can bind to the spike protein of SARS-CoV2 and inhibit viral infection. For instance, epigallocatechin gallate (EGCG) had an inhibitory effect, with an IC_{50} value of 0.32 µM against pseudovirus and an EC_{50} value of 24.08 against plaque formation of the live virus [39]. A total of 24 flavonoids exhibited antiviral entry activity with IC_{50} values ranging from 172.63 to 10.27 µM [40] which were higher than the IC_{50} values of compound **28**.

Despite the development of various peptides and small molecules as pan-coronavirus inhibitors targeting the spike protein in the past, these compounds specifically aimed at the fusion peptide of the spike protein, thereby blocking the cellular entry of coronaviruses by inhibiting membrane fusion, with low micromolar IC_{50} values [41–43].

With the objective of developing pan-coronaviral inhibitors that

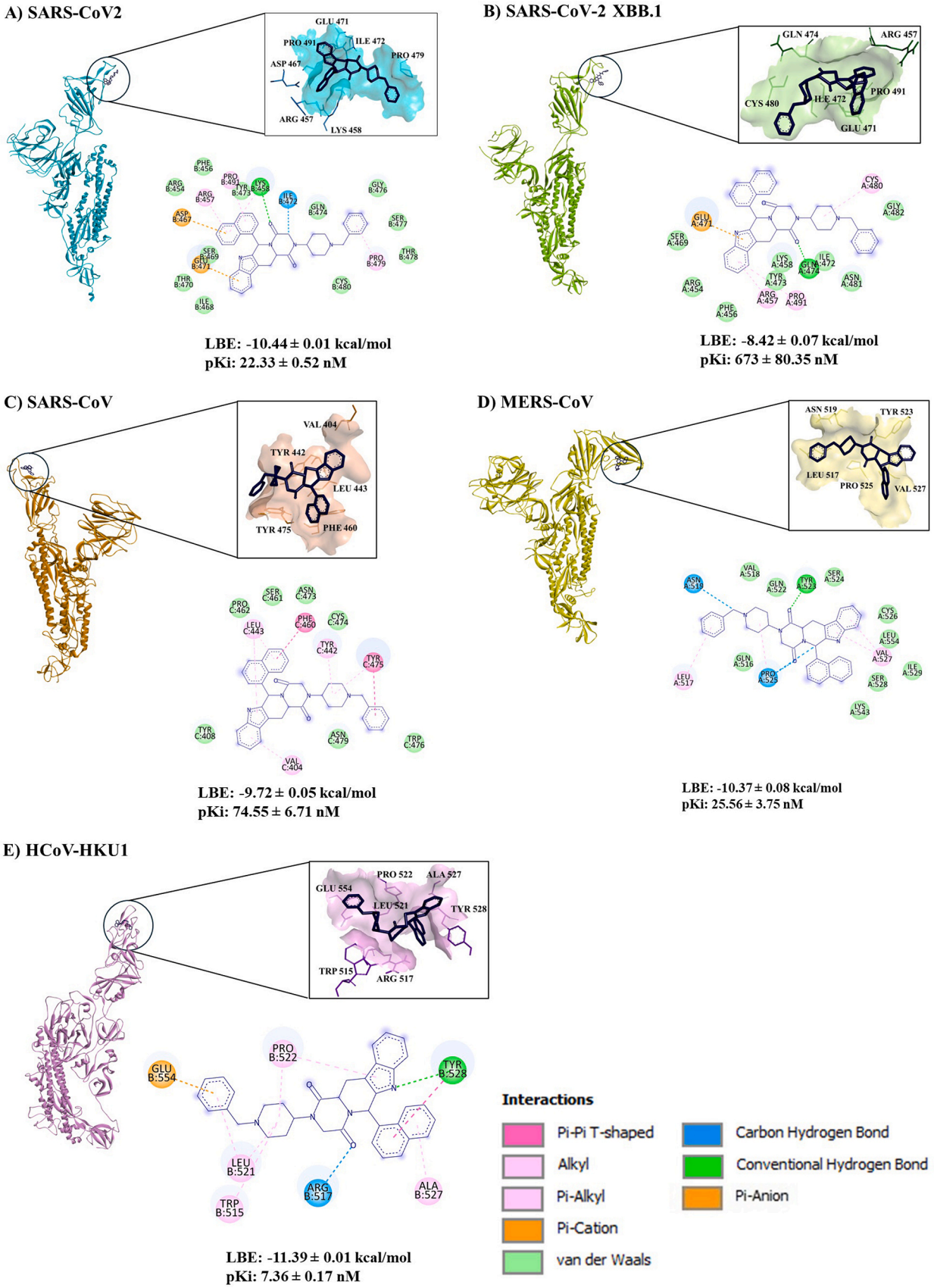

Fig. 6. The binding mode and 2D representation of compound **28** with the RBD of spike protein of (A) SARS-CoV-2 (PDB ID: 7bnn), (B) SARS-CoV-2 XBB.1 (PDB ID: 8iou), (C) SARS-CoV1 (PDB ID: 6acd), (D) MERS-CoV (PDB ID: 6nb3), and (E) HCoV-HKU1 (PDB ID: 8opo). These visualizations were generated using Discovery Studio Visualizer software (version v.24.1.0.23298). The lowest binding energies (LBE) and the predicted inhibition constant (pKi) of each compound were calculated using AutoDock 4.2.6.

specifically target the receptor-binding domain (RBD) of the spike protein, we initially conducted a sequence alignment for the RBD of SARS-CoV-2, SARS-CoV-2 XBB.1 (Omicron variant), SARS-CoV, MERS-CoV, and HCoV-HKU1. The Omicron variant exhibited the highest homology to wild-type SARS-CoV-2, while MERS-CoV showed the lowest. Subsequently, we employed microscale thermophoresis to examine the binding affinity of compound **28** to the RBD of the spike protein of these coronaviruses. The analysis confirmed that compound **28** successfully bound to the RBD of SARS-CoV-2, SARS-CoV-2 XBB.1, SARS-CoV, MERS-CoV, and HCoV-HKU1, with binding affinities correlating inversely with sequence homology identified in the alignment as indicated by an R value of −0.99 and a *p*-value of 0.001.

Previous studies have identified several hotspot residues on the RBD of SARS-CoV-2 critical for protein-protein or protein-ligand interactions, including R402, N439, N440, L441, K433, V444, G446, Y449, Y453, L452, L455, F456, T470, E471, I472, N481, E484, F486, N487, Y489, F490, Q493, Q498, P499, T500, N501, and Y505 [44–46]. A pharmacophore analysis based on the docking simulation revealed that compound **28** interacts with some of these hotspot residues, including F456, T470, and E471. Thus, the compound may interfere with the interaction between these residues and ACE2. The Omicron and wild-type RBDs shared similar overall structures, while the RBD of Omicron showed higher binding affinity for the ACE2 compared to the wild-type RBD [45]. Our molecular docking analysis revealed that compound **28** interacts with some of the hotspot residues in the RBDs of SARS-CoV-2 XBB.1, *i.e.*, F456, E471, I472 and N481, that may interfere with the interaction between RBD and ACE2. Moreover, molecular docking revealed that compound **28** may inhibit the HCoV-HKU1 virus entry through the interaction with the R517, L521, W515, Y528, and D529 hotspot residues [46,47] and SARS-CoV entry via the interaction with N473 and Y475 hotspot residues [46]. Although compound **28** does not interact with the hotspot residues of MERS-CoV [48], it still exert high affinities to the RBD based on their LBE of molecular docking and K_d values of microscale thermophoresis studies. Thus, the inhibitory effects of this compound towards MERS-CoV could take place by conformational changes of the RBD [49].

In summary, we present an *N*-heterocyclic natural product-derived compound as a broad-spectrum coronaviral entry inhibitor with low toxicity. By initially screening a large library of natural products, our strategy identified a highly promising agent. The presence of an *N*-heterocyclic structure in the active compound, despite the wide variety of other ZINC-derived starting structures, highlights the efficiency and specificity of our selection pathway, which effectively pinpointed this promising class of heterocycles from numerous candidates. This compound demonstrate the ability to protect cells from infection by both SARS-CoV-2 pseudoviruses and live viruses. Furthermore, *in silico* and *in vitro* studies revealed that they bind with high affinity to the RBD of SARS-CoV-2 XBB.1, SARS-CoV, MERS-CoV, and HCoV-HKU1. Thus, we conclude that compound **28** ((2 R,8S)-6-(1-benzylpiperidin-4-yl)-2-naphthalen-1-yl-3,6,17-triazatetracyclo[8.7.0.03,8.011,16]heptadeca-1(10),11,13,15-tetraene-4,7-dione) is a potential candidate for developing novel, potent pan-coronavirus entry inhibitors. Further investigations, including *in vivo* studies, will be necessary to validate these findings.

CRediT authorship contribution statement

Roland Schwarzer: Writing – review & editing, Methodology. **Hannah S. Schwarzer-Sperber:** Investigation. **Christian Meesters:** Writing – review & editing, Methodology. **Gerhard Bringmann:** Writing – review & editing, Writing – original draft, Conceptualization. **Kathrin Sutter:** Investigation. **Sara Abdelfatah:** Methodology, Conceptualization. **Nasim Shahhamzehei:** Writing – review & editing, Writing – original draft, Methodology, Investigation, Conceptualization. **Max Riedl:** Methodology, Investigation. **Ejlal A. Omar:** Investigation. **Thomas Efferth:** Writing – review & editing, Conceptualization.

Declaration of Competing Interest

The authors declare that they have no known competing financial interests or personal relationships that could have appeared to influence the work reported in this paper.

Acknowledgment

We are grateful to the financial support of Marc Strobel, Frankfurt a. M., Germany and CVC Philanthropy, Jersey.

References

[1] Y.C. Liu, R.L. Kuo, S.R. Shih, COVID-19: The first documented coronavirus pandemic in history, Biomed. J. 43 (2020) 328–333, https://doi.org/10.1016/j.bj.2020.04.007.
[2] WHO, Number of COVID-19 Cases Reported to WHO (Cumulative total) World, World Health Organization, 2024. ⟨https://data.who.int/dashboards/covid19/cases?n=o⟩.
[3] Y. Panahi, A.M. Gorabi, S. Talaei, F. Beiraghdar, A. Akbarzadeh, V. Tarhriz, et al., An overview on the treatments and prevention against COVID-19, Virol. J. 20 (2023) 1–29, https://doi.org/10.1186/s12985-023-01973-9.
[4] A. Yisimayi, W. Song, J. Wang, F. Jian, Y. Yu, X. Chen, et al., Repeated Omicron exposures override ancestral SARS-CoV-2 immune imprinting, Nature 625 (2024) 148–156, https://doi.org/10.1038/s41586-023-06753-7.
[5] C. Perrone, E. Fiabane, M. Maffoni, A. Pierobon, I. Setti, V. Sommovigo, et al., Vaccination hesitancy: to be vaccinated, or not to be vaccinated, that is the question in the era of COVID-19, Public Health Nurs. 40 (2023) 90–96, https://doi.org/10.1111/phn.13134.
[6] Z. Al-Aly, B. Bowe, Outcomes of SARS-CoV-2 reinfection, Res. Sq. (2022) 1–17.
[7] W.S. Ho, R. Zhang, Y.L. Tan, C.L.L. Chai, COVID-19 and the promise of small molecule therapeutics: are there lessons to be learnt? Pharmacol. Res. 179 (2022) 106201 https://doi.org/10.1016/j.phrs.2022.106201.
[8] J. Zhang, T. Xiao, Y. Cai, B. Chen, Structure of SARS-CoV-2 spike protein, Curr. Opin. Virol. 50 (2021) 173–182, https://doi.org/10.1016/j.coviro.2021.08.010.
[9] Y. Chen, Y. Guo, Y. Pan, Z.J. Zhao, Structure analysis of the receptor binding of 2019-nCoV, Biochem. Biophys. Res. Commun. 525 (2020) 135–140, https://doi.org/10.1016/j.bbrc.2020.02.071.
[10] N. Shahhamzehei, S. Abdelfatah, T. Efferth, In silico and in vitro identification of pan-coronaviral main protease inhibitors from a large natural product library, Pharmaceuticals 15 (2022) 1–19, https://doi.org/10.3390/ph15030308.
[11] S. Mhatre, S. Naik, V. Patravale, A molecular docking study of EGCG and theaflavin digallate with the druggable targets of SARS-CoV-2, Comput. Biol. Med. 129 (2021) 104137, https://doi.org/10.1016/j.compbiomed.2020.104137.
[12] A.V. Sadybekov, V. Katritch, Computational approaches streamlining drug discovery, Nature 616 (2023) 673–685, https://doi.org/10.1038/s41586-023-05905-z.
[13] X. Lin, X. Li, X. Lin, A review on applications of computational methods in drug screening and design, Molecules 25 (2020) 1–17, https://doi.org/10.3390/molecules25061375.
[14] F. Mölder, K.P. Jablonski, B. Letcher, M.B. Hall, C.H. Tomkins-Tinch, V. Sochat, et al., Sustainable data analysis with Snakemake, F1000Research 10 (2021) 33, https://doi.org/10.12688/f1000research.29032.1.
[15] E. Deelman, D. Gannon, M. Shields, I. Taylor, Workflows and e-science: an overview of workflow system features and capabilities, Future Gener. Comput. Syst. 25 (2009) 528–540, https://doi.org/10.1016/j.future.2008.06.012.
[16] K.H.D. Crawford, R. Eguia, A.S. Dingens, A.N. Loes, J.D. Bloom, K. Crawford, 2021, Pseudotyping lentiviral particles with SARS-CoV-2 Spike protein for neutralization assays V.2 Coronavirus Method Development Community 2021. https://doi.org/10.17504/protocols.io.br44m8yw..
[17] S.A. Almahboub, A. Algaissi, M.A. Alfaleh, M.Z. ElAssouli, A.M. Hashem, Evaluation of neutralizing antibodies against highly pathogenic coronaviruses: a detailed protocol for a rapid evaluation of neutralizing antibodies using vesicular stomatitis virus pseudovirus-based assay, Front. Microbiol. 11 (2020), https://doi.org/10.3389/fmicb.2020.02020.
[18] R.K.L. Lee, T.N. Li, S.Y. Chang, T.L. Chao, C.H. Kuo, M.Y.C. Pan, et al., Identification of entry inhibitors against delta and omicron variants of SARS-CoV-2, Int. J. Mol. Sci. 23 (2022), https://doi.org/10.3390/ijms23074050.
[19] C.S. Heilingloh, U.W. Aufderhorst, L. Schipper, U. Dittmer, O. Witzke, D. Yang, et al., Susceptibility of SARS-CoV-2 to UV irradiation, Am. J. Infect. Control 48 (2020) 1273–1275, https://doi.org/10.1016/j.ajic.2020.07.031.
[20] L. Schöler, V.T.K. Le-Trilling, M. Eilbrecht, D. Mennerich, O.E. Anastasiou, A. Krawczyk, et al., A novel In-Cell ELISA assay allows rapid and automated quantification of SARS-CoV-2 to analyze neutralizing antibodies and antiviral compounds, Front. Immunol. 11 (2020) 1–11, https://doi.org/10.3389/fimmu.2020.573526.
[21] V. Kuete, A.T. Mbaveng, E.C.N. Nono, C.C. Simo, M. Zeino, A.E. Nkengfack, et al., Cytotoxicity of seven naturally occurring phenolic compounds towards multifactorial drug-resistant cancer cells, Phytomedicine 23 (2016) 856–863, https://doi.org/10.1016/j.phymed.2016.04.007.

[22] E.-J. Seo, T. Efferth, Interaction of antihistaminic drugs with human translationally controlled tumor protein (TCTP) as novel approach for differentiation therapy, Oncotarget 7 (2016).
[23] M. Jerabek-Willemsen, C.J. Wienken, D. Braun, P. Baaske, S. Duhr, Molecular interaction studies using microscale thermophoresis, Assay. Drug Dev. Technol. 9 (2011) 342–353, https://doi.org/10.1089/adt.2011.0380.
[24] M. Zeino, M.E.M. Saeed, O. Kadioglu, T. Efferth, The ability of molecular docking to unravel the controversy and challenges related to P-glycoprotein - a well-known, yet poorly understood drug transporter, Investig. N. Drugs 32 (2014) 618–625, https://doi.org/10.1007/s10637-014-0098-1.
[25] Y. Yang, F. Peng, R. Wang, K. Guan, T. Jiang, G. Xu, et al., The deadly coronaviruses: The 2003 SARS pandemic and the 2020 novel coronavirus epidemic in China, J. Autoimmun. 109 (2020) 102434, https://doi.org/10.1016/j.jaut.2020.102434.
[26] A. Mermer, T. Keles, Y. Sirin, Recent studies of nitrogen containing heterocyclic compounds as novel antiviral agents: a review, Bioorg. Chem. 114 (2021) 105076, https://doi.org/10.1016/j.bioorg.2021.105076.
[27] C.M. Marshall, J.G. Federice, C.N. Bell, P.B. Cox, J.T. Njardarson, An update on the nitrogen heterocycle compositions and properties of U.S. FDA-approved pharmaceuticals (2013-2023), J. Med. Chem. (2024), https://doi.org/10.1021/acs.jmedchem.4c01122.
[28] E. Vitaku, D.T. Smith, J.T. Njardarson, Analysis of the structural diversity, substitution patterns, and frequency of nitrogen heterocycles among U.S. FDA approved pharmaceuticals, J. Med. Chem. 57 (2014) 10257–10274, https://doi.org/10.1021/jm501100b.
[29] M.M. Abdelshaheed, I.M. Fawzy, H.I. El-Subbagh, K.M. Youssef, Piperidine nucleus in the field of drug discovery, Futur J. Pharm. Sci. 7 (2021), https://doi.org/10.1186/s43094-021-00335-y.
[30] H. Ti, Z. Zhuang, Q. Yu, S. Wang, Progress of plant medicine derived extracts and alkaloids on modulating viral infections and inflammation, Drug Des. Dev. Ther. 15 (2021) 1385–1408, https://doi.org/10.2147/DDDT.S299120.
[31] D. Kang, Z. Fang, B. Huang, L. Zhang, H. Liu, C. Pannecouque, et al., Synthesis and preliminary antiviral activities of piperidine-substituted purines against HIV and influenza A/H1N1 infections, Chem. Biol. Drug Des. 86 (2015) 568–577, https://doi.org/10.1111/cbdd.12520.
[32] T.R. Freitas, R.M. Novais, I.A. Santos, D.O.S. Martins, A. Danuello, V. da Silva Bolzani, et al., In vitro antiviral activity of piperidine alkaloids from Senna spectabilis flowers on Chikungunya virus infection, Pharmacol. Rep. 74 (2022) 752–758, https://doi.org/10.1007/s43440-022-00381-0.
[33] M. Sharma, S.B. Bharate, N-benzyl piperidine fragment in drug discovery, ChemMedChem (2024), https://doi.org/10.1002/cmdc.202400384.
[34] Y.M. Ma, X.A. Liang, Y. Kong, B. Jia, Structural diversity and biological activities of indole diketopiperazine alkaloids from fungi, J. Agric. Food Chem. 64 (2016) 6659–6671, https://doi.org/10.1021/acs.jafc.6b01772.
[35] H. Gao, T. Zhu, D. Li, Q. Gu, W. Liu, Prenylated indole diketopiperazine alkaloids from a mangrove rhizosphere soil derived fungus Aspergillus effuses H1-1, Arch. Pharm. Res. 36 (2013) 952–956, https://doi.org/10.1007/s12272-013-0107-5.
[36] Y.H. Zhang, H.F. Du, Y.F. Liu, F. Cao, D.Q. Luo, C.Y. Wang, Novel anti-inflammatory diketopiperazine alkaloids from the marine-derived fungus Penicillium brasilianum, Appl. Microbiol. Biotechnol. 108 (2024), https://doi.org/10.1007/s00253-024-13026-4.
[37] K. Nishiuchi, H. Ohashi, K. Nishioka, M. Yamasaki, M. Furuta, T. Mashiko, et al., Synthesis and antiviral activities of neoechinulin B and its derivatives, J. Nat. Prod. 85 (2022) 284–291, https://doi.org/10.1021/acs.jnatprod.1c01120.
[38] W.S. Phutdhawong, 2,5-diketopiperazine derivatives as potential anti-influenza (H5N2) agents: synthesis, biological evaluation, and , and molecular docking study, Molecules (2022).
[39] D. Zhang, S. Hamdoun, R. Chen, L. Yang, C.K. Ip, Y. Qu, et al., Identification of natural compounds as SARS-CoV-2 entry inhibitors by molecular docking-based virtual screening with bio-layer interferometry, Pharmacol. Res. 172 (2021) 105820, https://doi.org/10.1016/j.phrs.2021.105820.
[40] J.R. Meng, J. Liu, L. Fu, T. Shu, L. Yang, X. Zhang, et al., Anti-entry activity of natural flavonoids against SARS-CoV-2 by targeting spike RBD, Viruses 14 (2022), https://doi.org/10.3390/v15010160.
[41] L. Guo, S. Lin, Z. Chen, Y. Cao, B. He, G. Lu, Targetable elements in SARS-CoV-2 S2 subunit for the design of pan-coronavirus fusion inhibitors and vaccines, Signal. Transduct. Target Ther. 8 (2023), https://doi.org/10.1038/s41392-023-01472-x.
[42] Q. Lan, L. Wang, F. Jiao, L. Lu, S. Xia, S. Jiang, Pan-coronavirus fusion inhibitors to combat COVID-19 and other emerging coronavirus infectious diseases, J. Med. Virol. 95 (2023), https://doi.org/10.1002/jmv.28143.
[43] S. Xia, L. Yan, W. Xu, A.S. Agrawal, A. Algaissi, C.T.K. Tseng, et al., A pan-coronavirus fusion inhibitor targeting the HR1 domain of human coronavirus spike, Sci. Adv. 5 (2019), https://doi.org/10.1126/sciadv.aav4580.
[44] L. Wang, Y. Wu, S. Yao, H. Ge, Y. Zhu, K. Chen, et al., Discovery of potential small molecular SARS-CoV-2 entry blockers targeting the spike protein, Acta Pharm. Sin. 43 (2022) 788–796, https://doi.org/10.1038/s41401-021-00735-z.
[45] J. Lan, X. He, Y. Ren, Z. Wang, H. Zhou, S. Fan, et al., Structural insights into the SARS-CoV-2 Omicron RBD-ACE2 interaction, Cell Res. 32 (2022) 593–595, https://doi.org/10.1038/s41422-022-00644-8.
[46] J. Lan, J. Ge, J. Yu, S. Shan, H. Zhou, S. Fan, et al., Structure of the SARS-CoV-2 spike receptor-binding domain bound to the ACE2 receptor, Nature 581 (2020) 215–220, https://doi.org/10.1038/s41586-020-2180-5.
[47] L. Xia, Y. Zhang, Q. Zhou, Structural basis for the recognition of HCoV-HKU1 by human TMPRSS2, Cell Res. (2024), https://doi.org/10.1038/s41422-024-00958-9.
[48] N. Wang, X. Shi, L. Jiang, S. Zhang, D. Wang, P. Tong, et al., Structure of MERS-CoV spike receptor-binding domain complexed with human receptor DPP4, Cell Res. 23 (2013) 986–993, https://doi.org/10.1038/cr.2013.92.
[49] S.R. Tzeng, C.G. Kalodimos, Protein activity regulation by conformational entropy, Nature 488 (2012) 236–240, https://doi.org/10.1038/nature11271.